

## Gate-tunable graphene spin valve

Sungjae Cho, Yung-Fu Chen,<sup>a)</sup> and Michael S. Fuhrer<sup>b)</sup>

Department of Physics and Center for Nanophysics and Advanced Materials, University of Maryland, College Park, Maryland 20742

(Received 16 July 2007; accepted 22 August 2007; published online 19 September 2007)

The authors perform nonlocal four-probe spin-valve experiments on graphene contacted by ferromagnetic Permalloy electrodes. They observe sharp switching and often sign reversal of the nonlocal resistance at the coercive field of the electrodes, indicating the presence of a spin current between injector and detector. The nonlocal spin-valve signal changes magnitude and sign with back-gate voltage, and is observed up to  $T=300$  K. The gate voltage variation of the spin-valve signal may result from quantum-coherent transport, as evidenced by Fabry-Pérot-like oscillations of the current. © 2007 American Institute of Physics. [DOI: 10.1063/1.2784934]

Graphene has been proposed as an ideal material for spin conduction;<sup>1,2</sup> it exhibits very long spin-scattering times<sup>2</sup> as a result of long electronic mean-free paths<sup>3,4</sup> and small spin-orbit coupling.<sup>5</sup> Graphene offers several advantages in lateral spin-valve structures: the absence of an energy gap allows electrical contacts from low Ohmic to tunneling to be engineered;<sup>2</sup> high current densities open the possibility of spin-transfer torque experiments in lateral spin valves; and an electrostatic gate may control transport. Here we demonstrate that a gate indeed can completely tune the nonlocal four-probe<sup>6</sup> spin-valve signal in a graphene device, changing its magnitude and even sign.

Our graphene samples are obtained by mechanical exfoliation<sup>7</sup> on 300 nm SiO<sub>2</sub>/Si substrates. We use optical microscopy to locate graphene and verify single-layer thickness<sup>8</sup> by comparing optical contrast with other samples on identical substrates which show the half-integer quantum Hall effect.<sup>3,4,9</sup> We estimate that all the samples discussed here are at most two graphene layers thick. Ferromagnetic Permalloy electrodes are formed by electron-beam lithography (EBL) followed by thermal evaporation; a second EBL step establishes contact to the Permalloy via Cr/Au electrodes.

Figure 1 describes the spin-valve device used for nonlocal four-probe experiments.<sup>6</sup> All spin-valve data shown here are taken on this device. (Other two-probe devices also showed spin-valve signals, including sign reversal, though the four-probe geometry offers more definitive evidence of a spin current.<sup>10</sup>) Figure 1(b) shows the gate voltage ( $V_g$ ) dependence of the resistivity  $\rho$  and conductivity  $\sigma$ . Similar to other single- and bilayer graphene devices,<sup>3,11</sup>  $\sigma(V_g)$  shows a broad minimum around  $4e^2/h$ , where  $e$  is the electronic charge and  $h$  is Planck's constant, increasing linearly with  $V_g$  away from the minimum at  $V_{\text{cnp}}$  [the charge neutrality point (CNP)]. The field-effect mobility  $\mu_{\text{FE}} = (1/c_g) |d\sigma/dV_g|$  is approximately  $2500 \text{ cm}^2/\text{V s}$ , where  $c_g = 1.15 \times 10^{-4} \text{ F/m}^2$  is the gate capacitance.

Figure 2(a) shows the four-probe nonlocal resistance  $R_{\text{nl}} = V_{\text{nl}}/I$  [see Fig. 1(c)] as a function of magnetic field  $B$  at  $V_g = +70$  V.  $R_{\text{nl}}$  is positive at large  $B$ . As  $B$  is swept to nega-

tive,  $R_{\text{nl}}$  remains positive as  $B$  crosses zero, then switches to a negative value at  $B \approx -150$  G before returning positive at  $B \approx -250$  G. Upon sweeping  $B$  positive, switching occurs at  $B = +150$  and  $+250$  G. This behavior is very similar to that observed in all-metal,<sup>6,12,13</sup> carbon nanotube (CNT),<sup>10</sup> and graphene<sup>2</sup> nonlocal spin-valves, particularly the sign change of  $R_{\text{nl}}$  when the current and voltage circuits are separated.<sup>2,10,13</sup> Hence, we identify these two magnetic fields as the coercive fields of  $F4$  and  $F3$  respectively.<sup>14</sup> The switching behavior may then be explained as follows: at high  $B$ ,  $F3$  preferentially injects its majority spin which diffuses to  $F4$  and is detected as an increase in the chemical potential of  $F4$ 's majority spin (since the magnetizations of  $F3$  and  $F4$  are parallel), resulting in positive  $R_{\text{nl}}$ . When  $F3$  and  $F4$  are antiparallel, the voltage reverses, and  $R_{\text{nl}}$  is negative.

Figures 2(b)–2(d) show the same measurement performed at different gate voltages and different electrode ar-

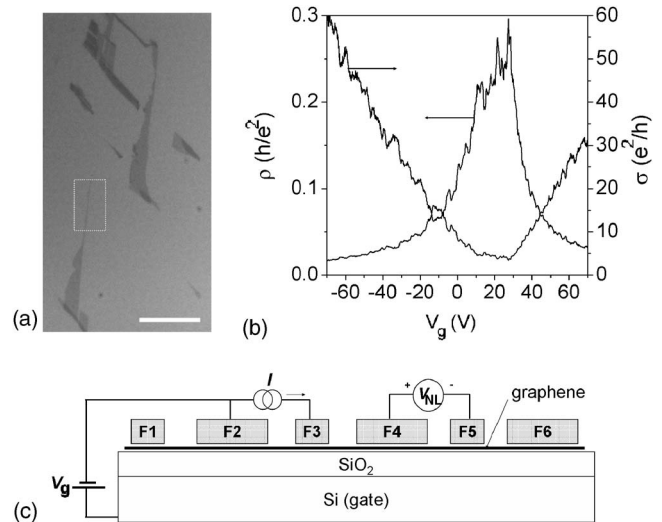


FIG. 1. Graphene spin-valve device. (a) Optical micrograph of graphene on SiO<sub>2</sub>/Si substrate. Scale bar is 10  $\mu\text{m}$ , white box shows the graphene flake used in this study, a strip approximately 350 nm wide. (b) Gate voltage ( $V_g$ ) dependence of four-probe resistivity  $\rho$  and conductivity  $\sigma$  at a temperature of 1.25 K. In this local resistivity measurement, electrodes  $F4$  and  $F5$  were used as voltage probes, and the current contacts were  $F3$  and  $F6$ . (c) Schematic of device layout, showing setup for nonlocal resistance measurement. Six ferromagnetic Permalloy electrodes  $F1$ – $F6$  were deposited on top of the graphene strip. To give different coercive fields,  $F1$ ,  $F3$ , and  $F5$  have dimensions of  $0.4 \times 15 \mu\text{m}^2$ , and  $F2$ ,  $F4$ , and  $F6$  are  $1.0 \times 3 \mu\text{m}^2$ . Spaces between all the electrodes are 450 nm.

<sup>a)</sup>Present address: Department of Physics, University of Illinois at Urbana-Champaign, 1110 West Green, Urbana, IL 61801-3080.

<sup>b)</sup>Author to whom correspondence should be addressed; electronic mail: mfuhrer@umd.edu

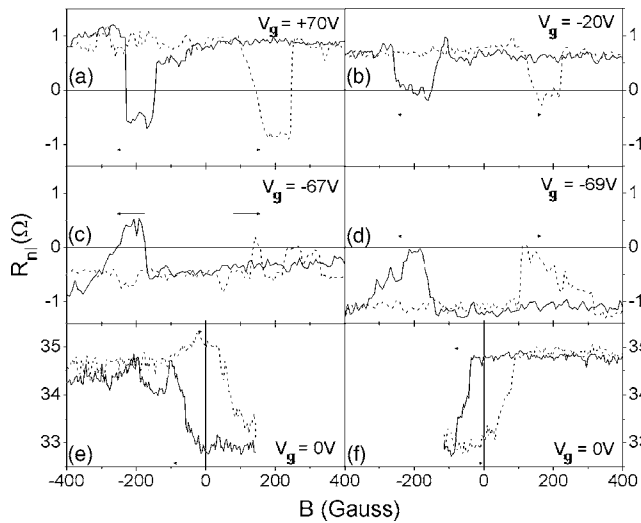


FIG. 2. Nonlocal resistance  $R_{nl}$  [see Fig. 1(c)] as a function of magnetic field measured at temperature  $T=20$  K with current  $I=100$  nA. In (a) and (b)  $F2, F3$  are current leads;  $F4, F5$  voltage leads. In (c) and (d),  $F4, F5$  are current leads;  $F2, F3$  voltage leads. Gate voltages are as follows:  $V_g = +70$  V in (a),  $V_g = -67$  V in (b),  $V_g = -20$  V in (c),  $V_g = -69$  V in (d). The nonlocal resistance switches sign upon sweeping magnetic field, which indicates that a spin current flows from electrodes  $F3$  to  $F4$ . Panels (e) and (f) show the memory effect measured at  $V_g = 0$  V.  $F1, F2$  are current leads;  $F3, F4$  are voltage leads. In all panels, dashed curves correspond to positive sweeping direction of magnetic field; solid curves, negative sweep direction.

rangements. In Figs. 2(b) and 2(d), the high- $B$  value is negative, and  $R_{nl}$  switches to near zero (or slightly positive) for  $B$  between the two coercive fields. The sign change is discussed further below. Figures 2(e) and 2(f) show the memory effect: two  $R_{nl}$  states can be observed at  $B=0$ , corresponding to the two possible magnetization states of the low-coercivity electrode.

First, we discuss whether  $R_{nl}$  arises due to charge current or spin current flowing between  $F3$  and  $F4$ . Ideally, charge current would flow only between  $F3$  and  $F2$ , eliminating contributions to  $R_{nl}$  from magnetoresistance of the ferromagnetic electrodes, the channel, or the electrode-channel interface. However, because  $R_{nl}$  is approximately three orders of magnitude smaller than the device resistance, it is possible that some charge current flows through a tortuous path from  $F3$  to  $F4$  and  $F5$ . We investigate this by measuring the gate voltage and temperature dependence of  $R_{nl}$ .

Figure 3(a) shows the gate voltage dependence of  $R_{nl}$  in the parallel and antiparallel states,  $R_{nl,p}$  and  $R_{nl,ap}$ , as well as their average value. Figure 3(b) shows the nonlocal spin-valve signal  $\Delta R$ .  $R_{avg}$ ,  $R_{nl,p}$ , and  $R_{nl,ap}$  all show a peak near the CNP ( $10 \text{ V} < V_g < 30 \text{ V}$ ), while  $\Delta R$  is near zero in this region. Well outside this region ( $V_g < -20$  or  $V_g > 40 \text{ V}$ ),  $R_{nl,p}$  and  $R_{nl,ap}$  have nearly equal magnitude and opposite signs ( $R_{avg}$  is nearly zero) and  $\Delta R$  is larger and shows quasi-periodic oscillations with  $V_g$ . The peak in  $R_{avg}(V_g)$  near the CNP suggests that charge current *does* flow in the region between  $F3$  and  $F4$  for these gate voltages. However,  $R_{avg}(V_g)$  is not simply proportional to  $\rho(V_g)$  but rather drops to near zero at large  $V_g$  while  $\rho(V_g)$  remains finite. Thus, the finite  $R_{avg}(V_g)$  near the CNP is likely due to the inhomogeneous nature of graphene near the CNP,<sup>9,15</sup> here, percolating electron and hole regions may cause a tortuous current path.

Away from the CNP,  $R_{avg}(V_g)$  drops to near zero, indicating small charge current. Yet,  $R_{nl,p}$  and  $R_{nl,ap}$  remain finite,

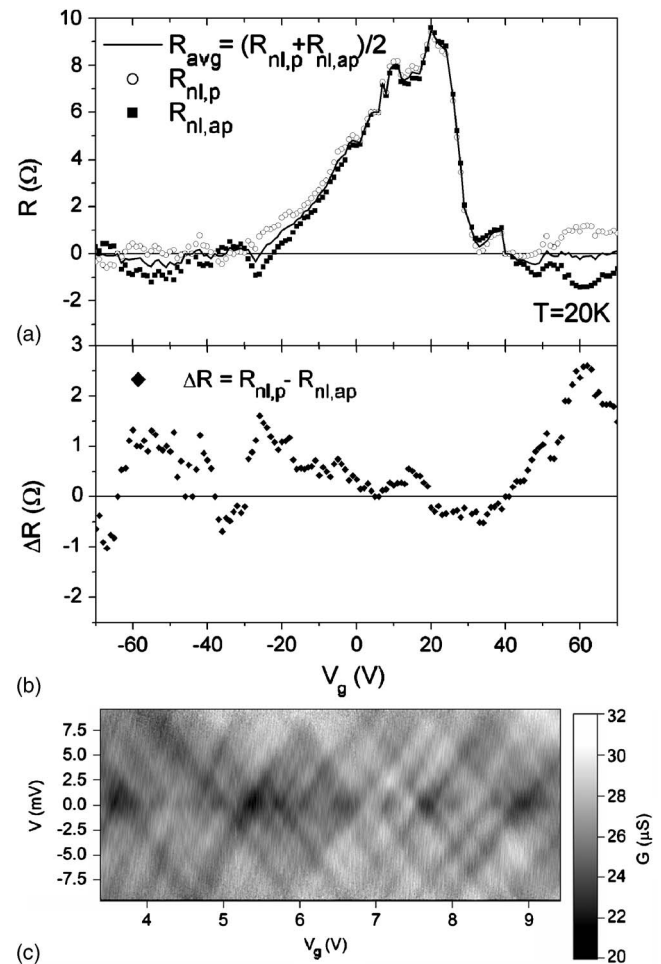


FIG. 3. (a) Resistance as a function of gate voltage for electrodes with magnetizations parallel ( $R_{nl,p}$ ), antiparallel ( $R_{nl,ap}$ ), and their average  $R_{avg} = (R_{nl,p} + R_{nl,ap})/2$ . (b) The spin valve signal  $\Delta R = R_{nl,p} - R_{nl,ap}$  as a function of gate voltage. In (a) and (b) the same electrode configuration is used as those of Figs. 2(a) and 2(b). (c) Gray-scale plot of two-probe differential conductance as a function of gate voltage  $V_g$  and drain voltage  $V$  for a similar graphene sample contacted by Permalloy electrodes with a spacing of 200 nm.

with nearly equal magnitude and opposite signs. This is as expected for a pure spin current flowing from  $F3$  to  $F4$ , and cannot be explained by a magnetoresistive signal arising from charge current between  $F4$  and  $F5$ . The Hall effect is another possible source of  $V_{nl}$ , however, the Hall voltage would be expected to grow large and switch sign near the CNP, rather than showing a peak.

Figure 4 shows the temperature dependence of  $R_{avg}$  and  $\Delta R$  for  $V_g = 0$ . Here,  $R_{avg}$  is finite similar to Fig. 3, but somewhat larger for this electrode configuration. The spin-valve signal  $\Delta R$  is seen to drop with temperature approximately as  $\Delta R \propto T^{-1}$ , while  $R_{avg}$  is much more weakly temperature dependent; again indicating a different origin for  $\Delta R$  and  $R_{avg}$ . The inset shows a measurement at 300 K performed at higher current; the spin-valve signal can still be observed.

We now discuss the origins of the variations and sign changes of the nonlocal spin-valve signal  $\Delta R(V_g)$ . Oscillation of the spin-valve signal with  $V_g$  due to spin-orbit coupling has been proposed as the basis of a spin transistor.<sup>16</sup> However, the spin-orbit coupling in graphene is expected to be very small,<sup>5</sup> and this effect should not be observable.<sup>17</sup> Oscillations of the spin-valve signal have also been observed when the spin current flows through a resonant quantum

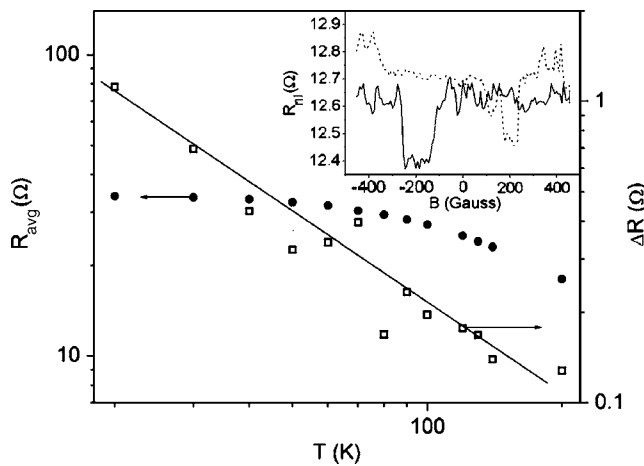


FIG. 4. Average resistance  $R_{\text{avg}}$  (solid circles) and spin valve signal  $\Delta R$  (open squares) as a function of temperature at  $V_g=0$  V and  $I=100$  nA. The solid line shows a power law with exponent  $-1$ . The inset shows the non-local resistance  $R_{\text{nl}}$  as a function of field at  $T=300$  K and  $I=3$   $\mu\text{A}$ . Dashed curve is positive sweep direction of magnetic field; solid curve, negative sweep direction. The electrodes used for the spin-valve data in main panel and inset are the same as those of Figs. 2(e) and 2(f).

state, either due to Coulomb blockade<sup>18</sup> or resonant tunneling.<sup>19</sup> Here, it is possible for the injected current to have polarization opposite the majority spin of the injecting electrode, resulting in reversal of the signs of the two-probe,<sup>18</sup> and, in principle, the nonlocal, spin-valve signal. It is evident from Fig. 1(b) that the sample is not in the Coulomb blockade regime, however,  $\rho(V_g)$  shows quasiperiodic oscillations. We examined similar oscillations in another similar graphene sample in a two-probe geometry [Fig. 3(c)]. In the gray-scale plot of differential conductance versus  $V_g$  and drain voltage  $V$ , conductance maxima and minima occur along the diagonal lines. In CNTs (Ref. 19 and 20) and in graphene<sup>21</sup> such behavior is attributed to Fabry-Pérot interference of electronic states partially reflected from the electrodes. Thus, we conclude that there is coherent transport of electrons at least across the length of the sample. The four-probe geometry is significantly more complicated, since there are multiple interfaces which could give rise to interference. Still, it is reasonable that quantum interference effects are responsible for the prominent oscillations in the four-probe resistivity [Fig. 1(b)], and for the observed changes in magnitude and sign of the spin-valve signal with gate voltage [Fig. 3(b)].

Tombros *et al.* have also reported four-probe nonlocal spin-valve measurements on graphene samples but did not report significant dependence of the spin-valve signal on gate voltage.<sup>2</sup> We believe this is possibly due to the fact that their measurements are carried out on larger samples, at higher  $T$  (gate voltage dependence was only reported at room  $T$ ), and higher currents, which would tend to average out interference effects on the spin-valve signal. In our experiment the average  $\Delta R(V_g)$  is positive [Fig. 3(b)], as expected, and we have observed only positive  $\Delta R$  at  $T=300$  K, though we have not made a detailed study of  $\Delta R(V_g)$  at  $T > 20$  K.

In conclusion, we have observed the nonlocal resistance arising from a spin current in graphene in a nonlocal four-probe measurement. The spin-valve signal varies with gate voltage in magnitude and sign, possibly due to quantum-coherent transport through graphene, which is also evidenced by Fabry-Pérot-like interference patterns observed in a similar sample, and oscillations in the four-probe resistivity of the spin-valve sample. Control of pure spin currents in graphene opens possibilities to examine theoretically predicted phenomena such as the spin Hall effect<sup>5</sup> and half-metallicity in graphene ribbons.<sup>22</sup> Because of the high current-carrying capability and long mean-free path at room temperature,<sup>3,4</sup> graphene is also an excellent candidate for room-temperature spintronics applications.

This work has been supported by the U.S. ONR grant N000140610882, NSF grant CCF-06-34321, and the UMD-NSF-MRSEC grant DMR-05-20471.

- <sup>1</sup>E. W. Hill, A. K. Geim, K. Novoselov, F. Schedin, and P. Blake, *IEEE Trans. Magn.* **42**, 2694 (2006).
- <sup>2</sup>N. Tombros, C. Jozsa, M. Popinciuc, H. T. Jonkman, and B. J. van Wees, *Nature (London)* **448**, 571 (2007).
- <sup>3</sup>K. S. Novoselov, A. K. Geim, S. V. Morozov, D. Jiang, M. I. Katsnelson, I. V. Grigorieva, S. V. Dubonos, and A. A. Firsov, *Nature (London)* **438**, 197 (2005).
- <sup>4</sup>Y. Zhang, Y.-W. Tan, H. L. Stormer, and P. Kim, *Nature (London)* **438**, 201 (2005).
- <sup>5</sup>C. L. Kane and E. J. Mele, *Phys. Rev. Lett.* **95**, 226801 (2005).
- <sup>6</sup>F. J. Jedema, A. T. Filip, and B. J. van Wees, *Nature (London)* **410**, 345 (2001).
- <sup>7</sup>K. S. Novoselov, D. Jiang, F. Schedin, T. J. Booth, V. V. Khotkevich, S. V. Morozov, and A. K. Geim, *Proc. Natl. Acad. Sci. U.S.A.* **102**, 10451 (2005).
- <sup>8</sup>D. S. L. Abergel, A. Russell, and V. I. Fal'ko, *Appl. Phys. Lett.* **91**, 063125 (2007).
- <sup>9</sup>S. Cho and M. S. Fuhrer (<http://xxx.lanl.gov/abs/0706.1597>).
- <sup>10</sup>N. Tombros, S. J. van der Molen, and B. J. van Wees, *Phys. Rev. B* **73**, 233403 (2006).
- <sup>11</sup>K. S. Novoselov, E. McCann, S. V. Morozov, V. I. Fal'ko, M. I. Katsnelson, U. Zeitler, D. Jiang, F. Schedin, and A. K. Geim, *Nat. Phys.* **2**, 177 (2006).
- <sup>12</sup>F. J. Jedema, M. S. Nijboer, A. T. Filip, and B. J. van Wees, *J. Supercond.* **15**, 27 (2002).
- <sup>13</sup>S. Garzon, I. Zutic, and R. A. Webb, *Phys. Rev. Lett.* **94**, 176601 (2005).
- <sup>14</sup> $F_2$  and  $F_5$  are ferromagnetic and have similar coercivities to  $F_4$  and  $F_3$ , respectively; however, this results in similar overall behavior as the case with only  $F_3$  and  $F_4$  ferromagnetic (Refs. 2 and 10).
- <sup>15</sup>S. Adam, E. H. Hwang, V. M. Galitski, and S. D. Sarma (<http://arxiv.org/abs/0705.1540>).
- <sup>16</sup>S. Datta and B. Das, *Appl. Phys. Lett.* **56**, 665 (1990).
- <sup>17</sup>A. De Martino and R. Egger, *J. Phys.: Condens. Matter* **17**, 5523 (2005).
- <sup>18</sup>S. Sahoo, T. Kontos, J. Furer, C. Hoffmann, M. Gräber, and C. Schönberger, *Nat. Phys.* **1**, 99 (2005).
- <sup>19</sup>H. T. Man, I. J. W. Wever, and A. F. Morpurgo, *Phys. Rev. B* **73**, 241401 (2006).
- <sup>20</sup>W. Liang, M. Bockrath, D. Bozovic, J. H. Hafner, M. Tinkham, and H. Park, *Nature (London)* **411**, 665 (2001).
- <sup>21</sup>F. Miao, S. Wijeratne, Y. Zhang, U. C. Coskun, W. Bao, and C. N. Lau, *Science* **317**, 1530 (2007); S. Cho, Y.-F. Chen, and M. S. Fuhrer, [arXiv:cond-mat/0706.1597](http://arxiv.org/abs/cond-mat/0706.1597)
- <sup>22</sup>Y.-W. Son, M. L. Cohen, and S. G. Louie, *Nature (London)* **444**, 347 (2006).